ACS EARTH AND SPACE CHEMISTRY

Article

http://pubs.acs.org/journal/aesccq

Mineral Surface Rearrangement at High Temperatures: Implications for Extraterrestrial Mineral Grain Reactivity

Helen E. King,*[,†,‡,§] Oliver Plümper,[∥] Christine V. Putnis,[†,⊥] Hugh St. C. O'Neill,[#] Stephan Klemme,[†] and Andrew Putnis[†,±]

[†]Institut für Mineralogie, University of Münster, Corrensstrasse 24, 48149 Münster, Germany

[‡]Department of Geology and Geophysics, Yale University, 210 Whitney Avenue, New Haven, Connecticut 06511, United States

[§]Department of Chemistry, University College London, 20 Gordon Street, London WC1H 0AJ, United Kingdom

[∥]Department of Earth Sciences, Utrecht University, Budapestlaan 4, 3584 CD Utrecht, The Netherlands

[⊥]Department of Chemistry, Curtin University, Kent Street, Perth 6845, Australia

[#]Research School of Earth Sciences, The Australian National University, Canberra, ACT 2601, Australia

[±]The Institute for Geoscience Research (TIGeR), Curtin University, P.O. Box U1987, Perth 6845, Australia

ABSTRACT: Mineral surfaces play a critical role in the solar nebula as a catalytic surface for chemical reactions and potentially acted as a source of water during Earth's accretion by the adsorption of water molecules to the surface of interplanetary dust particles. However, nothing is known about how mineral surfaces respond to short-lived thermal fluctuations that are below the melting temperature of the mineral. Here we show that mineral surfaces react and rearrange within minutes to changes in their local environment despite being far below their melting temperature. Polished surfaces of the rock and planetary dust-forming silicate mineral olivine ($(Mg,Fe)_2SiO_4$) show significant surface reorganization textures upon rapid heating resulting in surface features up to 40 nm in height observed after annealing at 1200 °C. Thus, high-temperature fluctuations should provide new and highly reactive sites for chemical reactions on nebula mineral particles. Our results also may help to explain discrepancies between short and long diffusion profiles in experiments where diffusion length scales are of the order of 100 nm or less.

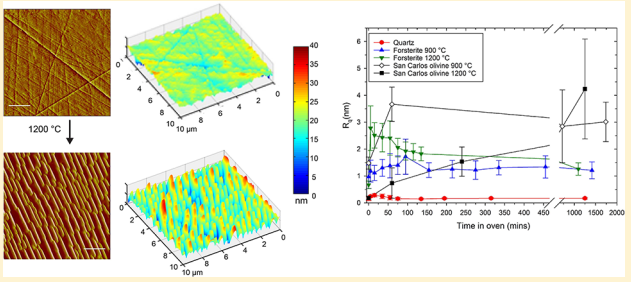

KEYWORDS: *Mineral surface reconstruction, solar nebula, gas adsorption, experiments, atomic force microscopy AFM*

INTRODUCTION

Whether life can be supported on a planet depends on its budget of the volatile elements. Hence, understanding how volatiles came to Earth and what the initial volatile inventory of terrestrial planets was is important to understand the conditions under which prebiotic chemistry and the potential emergence of life can occur. There have been extensive investigations into the source of volatiles on Earth and other terrestrial planets. Particularly, the origin of Earth's water, critical for the development of life, remains an unresolved issue.[1] The Earth could have accreted water throughout its formation.[2] During this time the extraterrestrial delivery via comets and/or asteroids has become a favored mechanism due to the comparion of the deuterium-to-hydrogen ratio (D/H) of the terrestrial ocean water and that found in situ during the Rosetta comet mission.[3,4] However, recent computational and experimental studies have repeatedly demonstrated that gas adsorption onto mineral dust grains in the solar nebula could also be a source of volatiles.[5−8] This is supported by new D/H isotopic data from a potential primordial reservoir retained in terrestrial lavas, which indicate a nebula origin of water delivered via adsorption to dust grains.[9] In all of these mechanisms, at least part of the water delivered was most likely adhered to the mineral matrix of the delivering body, whether comets, asteroids, or interplanetary dust particles. The extent to which these surface processes make a significant impact on volatile budgets depends on mineral grain surface structures that control reactivity. In addition to the delivery of volatiles, mineral surfaces in the solar nebula provide catalytic sites for a range of reactions including organic molecule formation.[10] Thus, understanding the processes occurring at mineral surfaces is critical for unravelling the chemical processes occurring within solar nebulae and during planetary accretion.

Olivine, a Mg−Fe silicate mineral, has been identified in a diverse range of environments in the universe including planets, satellites, comets, asteroids, and interplanetary dust particles to luminous quasars.[11] Thus, olivine mineral surfaces are expected

Received: December 21, 2016
Revised: March 6, 2017
Accepted: March 6, 2017
Published: March 31, 2017

DOI: 10.1021/acsearthspacechem.6b00016
ACS Earth Space Chem. 2017, 1, 113−121

to be present in many different environments, making the understanding of their catalytic and adsorbing surfaces in the nebula of prime importance. The first olivine to condense from the solar nebula has a composition close to forsterite (Mg_2SiO_4). Hence pure forsterite has been extensively studied for evaporative isotope fractionation effects controlled by surface processes.[12−14] However, olivine in the nebula becomes progressively more Fe rich as partially oxidized Fe also condenses from the nebula and subsequently is incorporated into the forsterite mineral grains.[15,16] Reflectance spectra of asteroids and nebula dust support this showing that most of the olivine contains small amounts of Fe.[17] Despite this, no studies have examined how the presence of Fe in forsteritic olivine affects surface-related processes.

One potential source of water on planets like Earth is the strong chemisorption of hydroxyl species onto olivine surfaces. In this mechanism, structural defects, such as surface steps and corners, are required to provide highly reactive sites where chemisorption is energetically favorable.[7] The typical dust grain formation processes of dust particle agglomeration[18,19] would be expected to produce defective surfaces, as could fast cooling after intense, short-lived bursts of heat that are proposed to form large mineral grains.[20,21] However, these defect-rich surfaces, fundamental to any extraterrestrial adsorption process, may also be eradicated by these high-temperature annealing events. Although the formation of etch-pits has been documented during transient incursions into the evaporation regime (above 1400 °C under solar nebula conditions) forming defect-rich and hence more reactive surface sites,[13,22] nothing is known about the effects of similar scale short-lived thermal fluctuations below this temperature. To date there are no experiments that investigate what occurs at a mineral surface below its melting temperature but at high enough temperatures that atoms can still be highly mobile due to diffusion. To answer this crucial question, we have investigated how polished surfaces of both pure forsterite and San Carlos olivine ($Mg_{0.8}Fe_{0.2}SiO_4$) crystals react to short-lived bursts of increased temperature by monitoring nanoscale changes in surface topography using atomic force microscopy (AFM). The processes occurring at these olivine surfaces are compared to a quartz crystal surface as an example of a less reactive mineral. We observed that olivine mineral surfaces react within minutes at temperatures as low as 900 °C, producing highly reconstructed surfaces that can provide potential reactive sites for gas adsorption.

EXPERIMENTAL SECTION

As it has been suggested that surface Fe provides the most important catalytic sites for olivine,[10] for comparison experiments were conducted on pure synthetic forsterite (Mg_2SiO_4) and natural San Carlos olivine ($Mg_{1.8}Fe_{0.2}SiO_4$), as well as quartz (SiO_2) as a reference silicate mineral. Samples were annealed at 900 and 1200 °C, temperatures at which olivine undergoes significant sublimation in vacuum (>1400 °C)[12] and within the temperature range expected to affect grains during the short pulses of shock heating (up to ∼1900 °C; see ref 23 for discussion). Randomly oriented surfaces were examined to produce a clearer image of olivine reactivity as the (010), (001), and (100) surfaces previously studied in experiments[8,13] would not be the only surfaces present on the fast cooled or fractal olivine dust particles present in the nebula.

Experimental Methods. Cubes (1 × 1 × 0.5 cm) of the synthetic forsterite (Mg_2SiO_4), gem quality San Carlos olivine ($Mg_{1.8}Fe_{0.2}SiO_4$), and quartz (SiO_2) crystals were cut from larger slices that had been polished on one face using SYTON. The forsterite was synthesized using the Czochralski method; a full chemical analysis is given in ref 24. Parts of the same crystal have been used previously in diffusion experiments with results consistent with good crystallinity with no evidence for extended defects that could cause fast diffusion pathways.[24,25] After polishing, the samples were sonicated in acetone for 30 min. The surfaces were subsequently dried with a Kimwipe and blown with compressed air. For muffle oven experiments with synthetic forsterite and quartz at 900 or 1200 °C, the oven was heated to the required temperature and then the crystals were placed into the oven in a Pt crucible (∼10 mm high with wall thickness of 0.5 mm) with the polished face upward. The controlling thermocouple in the oven returned to temperature within 5 min, suggesting that the crystal reached thermal equilibrium in even shorter times due to its low thermal mass, which is insignificant compared to that of the surrounding oven, and the thermal diffusivity of olivine.[26] The crystal was removed after 10 min and analyzed then placed back into the oven. Further analysis of the surface structure was conducted at 20 min intervals (total time in oven: 2 h) before leaving the crystal in the oven overnight. Each time the crystal was removed from the oven it was left to cool in air on the benchtop for approximately 2 min and then immediately imaged by AFM, which took approximately 30 min. The images were consistent over the 30 min, indicating that there was minimal reaction of the surface with the atmosphere during this time. By cooling the crystal prior to imaging, we minimized distortion of the AFM image due to expansion of the tip cantilever. After scanning, the crystal was put back into the oven for further reheating to study the development of surface structure as a function of time on the same sample.

To prevent Fe oxidation in the San Carlos olivine, these samples were annealed in a conventional vertical high-temperature furnace (Gero GmbH, Germany), which was equipped with gas mixing facilities. We used a 1:1 CO/CO_2 gas mixture in all experiments with the exception of the oxidation test experiment where a ratio of 1:9 CO/CO_2 gas was used. The furnace was sealed and air was purged using a continuous flow of pure CO_2 while the furnace was heated to 900 °C (typically taking up to an hour to stabilize). After the oven had stabilized in temperature at 900 °C, the gas mix was adjusted to the required ratio and left for a further 30 min to ensure that the atmosphere in the furnace had equilibrated. At this point, the sample cube was inserted by suspending it within a loose basket of Pt wire from a drop-quench sample holder of the type described in ref 27. For the 1200 °C experiments, the furnace was heated from 900 °C after the crystal had been placed inside, taking approximately 100 min to reach the required temperature. The crystals were quenched by dropping them into an air-cooled metal trap directly below the furnace that was expected to have a similar gas atmosphere. Samples were extracted at longer intervals (after 60 min, 240 min, and overnight) than the muffle oven experiments to minimize exchange of the internal gas with the atmosphere during sample placement and extraction. As for the muffle oven experiments, the crystals were left to cool in the trap for approximately 2 min before being removed and immediately imaged with the AFM. Within the 30 min required to scan the surface, the textures remained consistent indicating that there was minimal further reaction of the surface within this time. After scanning, the

DOI: 10.1021/acsearthspacechem.6b00016
ACS Earth Space Chem. 2017, 1, 113−121

same crystal was immediately placed back into the furnace for the next stage of the experiment.

Atomic Force Microscopy. Nanoscale imaging of the surface before and after annealing was conducted using a Nanoscope III Multimode AFM (Digital Instruments, Bruker) functioning in contact mode. AFM images of 10 randomly selected areas were collected with a scanning frequency of 3 Hz using Si_3N_4 tips (Bruker, tip model NP-S20) with spring constants of 0.12 and 0.58 N/m. Deflection and height images of 5 × 5 and 10 × 10 μm areas of the surfaces were collected and analyzed using the NanoScope software (Version 5.31r1). Surface roughness measurements/calculations of the AFM images were performed using the inbuilt functions of the Nanoscope software. R_q, the standard deviation of height (Z) within an allotted 1 × 1 μm area, was calculated using

$$R_q = \sqrt{\frac{\sum (Z_i)^2}{N}} \quad (1)$$

where Z_i is the height of each individual point and N is the number of points within the specified area for each of the 20 images taken from each surface. By using a 1 × 1 μm area we avoided any changes in the density of the original polishing scratches in our calculations and additional particles that were sometimes found on the surfaces. These roughness values were then averaged and the standard deviation (1σ) calculated for the variation across the surface.

Raman Spectroscopy. After annealing the 532 nm line of a 14 mW Nd:YAG laser in a high resolution Jobin Yvon Xplora Raman microscope was used to examine the sample surface. To limit the penetration of the laser beam into the sample, but maintain a large enough peak intensity above the background noise, a hole size of 300 μm was used. Drift of the Raman microscope during the measurement session was corrected using the first order Raman band of a silicon wafer, which is present at 520.7 cm^{-1}. After being scattered by the sample, the Raman light was collected in a 180° backscattering geometry, passed through a 100 μm entrance slit, and dispersed by a grating of 1800 grooves/mm before reaching the charge-coupled device detector.

Electron Backscatter Diffraction. Electron backscattered diffraction (EBSD) patterns were taken before and after annealing in order to examine crystalline continuity across the surface. EBSD patterns arise from cones of backscattered electrons that obey Bragg's law and are emitted from a tilted sample surface. EBSD is a surface sensitive technique that is used to examine orientation of samples with long-range order, thus crystalline minerals.[28] The EBSD analysis was carried out in a JEOL JSM-6610LV scanning electron microscope (SEM), operating at 15 nA and 20 kV. The SEM is equipped with a secondary electron detector and electron backscatter detector as well as energy dispersive X-ray (EDX) detector for elemental analysis. EBSD analyses were conducted using a single crystal mounted on a 70° tilted stage at a working distance of 15 mm. EBSD patterns were collected on a phosphor screen and indexed using the CHANNEL 5 software by HKL Technology.

RESULTS AND DISCUSSION

Experiments with Synthetic Forsterite (Mg_2SiO_4). AFM nanoscale analysis of the sample surfaces after annealing at increased temperature (900 and 1200 °C) demonstrated two important features. First, during the course of experiments at both temperatures discrete particles were observed to have formed along large scratches (0.9 μm width and ∼10 nm deep). These particles grew in size from an average of 90 nm diameter after 5 min in the oven to 140 nm after 1500 min, corresponding with a decrease in the overall number of particles from an average of 200 to 20 within each 100 μm^2 scanned area. On the submicron AFM scale, the particles could be seen aligning and filling scratches, often producing features that were higher than the rest of the surface (Figure 1a). SEM imaging during EBSD analysis showed that the larger particles had well-defined crystal faces implying that the phase formed was possibly crystalline. Raman analysis of the particles produced no Raman peaks above the background, however, EDX analysis showed a large Pt peak associated with the particles. Therefore, these particles were omitted from further image analysis and only sections of the images where these particles were not detected were examined for surface roughness. SEM-EDX analysis of the areas between the particles showed no evidence for Pt contamination and the EBSD patterns between the Pt particles were consistent with forsterite. Mobility of Pt at these temperatures is expected from transport of Pt through the gas phase as oxidized species,[29] before decomposing back to Pt metal at the sample surface.[30]

Second, the forsterite surface itself demonstrated a temperature-dependent change in surface topography during the course of the experiment (Figure 2). Initial polishing scratches became increasingly less distinguishable during the course of the experiment at 900 °C (Figure 2b). The surface between the scratches shows a slight change in topography, which is also visible in the plot of R_q with time (Figure 3). Changes in roughness increase slowly over the first 50 min on the synthetic forsterite surface at 900 °C before establishing a consistent roughness across the surface. The stability of R_q within the standard deviation over the course of many measurements indicates that the surface had reached a steady-state configuration. The height of the surface undulations only reaches a few nanometers above the initial surface height, as shown in Figure 2 (compare a and b) by the end of the experiment. In contrast, experiments at 1200 °C show a sharp increase in the measured roughness within the first 10 min of annealing from 0.7 nm before the experiment to 2.8 nm (Figure 3). Comparison with the initial surface features indicates that the scratches do not change in depth with time, remaining approximately 10 nm deep. However, the rest of the surface between the scratches developed an undulating structure that is aligned across the area of the surface images (5 or 10 μm), regardless of initial scratch orientation (Figure 2c). This roughness slowly coarsens with time, evident as a gradual decrease in R_q from 2.8 after 10 min to 1.2 nm at the end of the experiment (1000 min at 1200 °C), where the roughness is again uniformly distributed across the surface.

Experiments with San Carlos olivine ($Mg_{0.8}Fe_{0.2}SiO_4$). Experiments with San Carlos olivine were conducted using a 1:1 CO/CO_2 gas mix to ensure that oxidation did not play a role in changes to surface features. In one set of experiments with a sintered alumina rod that had not previously been used, a new layer of material was observed to form on the olivine surface at both 900 and 1200 °C. During these experiments triangular particles nucleated on the surface within the first 10 min of the experiment and continued to grow throughout the experiment until they had completely covered the reacting surface (Figure 1b). These particles had an average length of 0.7 μm and a height of ∼5 nm. Analysis with Raman spectroscopy produced no measurable Raman peaks and

DOI: 10.1021/acsearthspacechem.6b00016
ACS Earth Space Chem. 2017, 1, 113−121

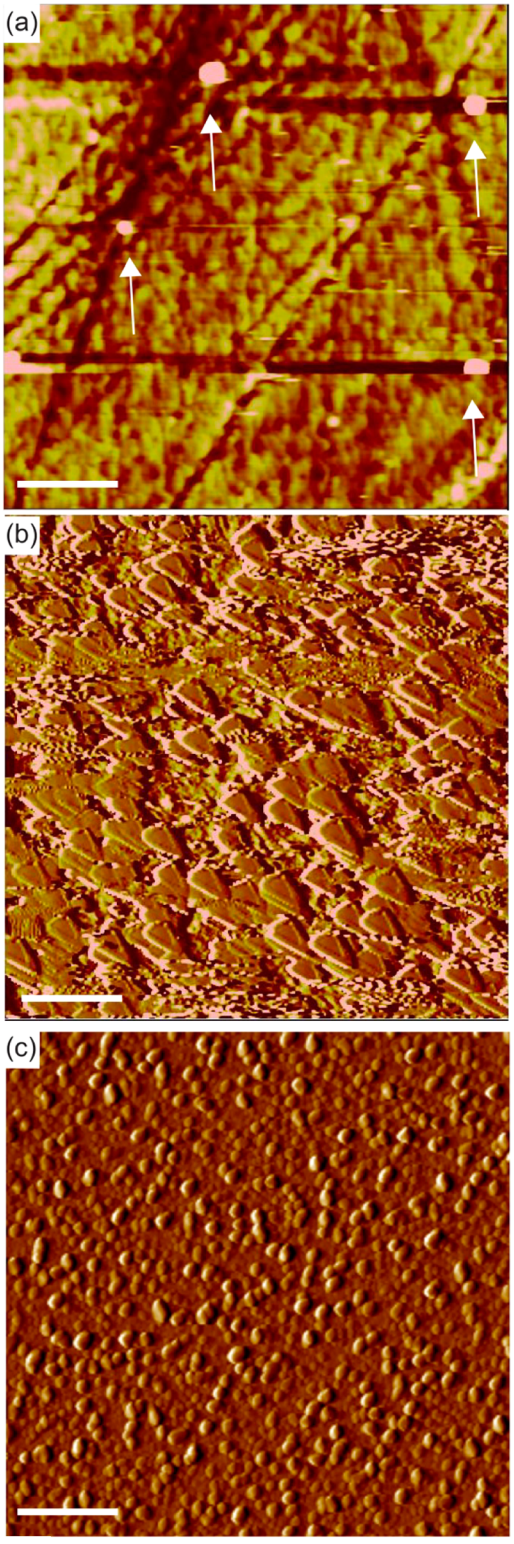

Figure 1. (a) AFM height image of the synthetic forsterite surface at 1200 °C showing the formation of Pt particles (white arrows) along scratches. Height of the Pt particles is ~15 nm. (b) AFM deflection image of triangular particles formed on a San Carlos olivine surface during a mixed gas experiment with a new alumina sample holder. (c) AFM deflection image of surface features produced during heating within a gas mixture of 10:90 CO/CO_2 on olivine at 900 °C. Scale bar in all images: 2 μm.

EBSD analysis showed no clear Kikuchi lines indicating that the new phase is Raman inactive and completely obscures the underlying mineral surface. EDX elemental analysis and considerations of the experimental set up, that is, use of a new alumina rod, indicate that the newly formed phase is alumina. Therefore, only data obtained using aged alumina rods have been used for data reduction for these experiments. In these experiments, there was no evidence for the formation of the triangular alumina phase.

The most significant rearrangement of the sample crystal surface at high temperature was observed with the San Carlos olivine. As can be seen from Figure 4a, the original polished surfaces of San Carlos olivine typically had a higher initial surface roughness (synthetic forsterite, 0.81 nm ± 0.3; San Carlos olivine, 1.49 nm ± 0.4). However, exposure of the surface to 900 °C temperatures produced very similar undulating surface features to those observed with synthetic forsterite at 1200 °C (compare Figures 2c and 4b) but were larger in overall height, producing a large R_q value (Figure 3). For the San Carlos olivine, these features were observed after 135 min of annealing, unlike synthetic forsterite where they were observed within the first 10 min of exposure to 1200 °C. As in the two synthetic forsterite experiments, the measured roughness of San Carlos olivine at 900 °C initially increased before coarsening, producing a decline in the measured roughness parameter (R_q) by the end of the experiment as seen in Figure 3. As for the 900 °C experiments with synthetic olivine, the roughness remained constant within the standard deviation over the last two measurements (Figure 3) indicating that the system had reached a steady-state configuration. Experiments with San Carlos olivine at 1200 °C showed the most extensive surface reconstruction where large undulations between 9 and 38 nm height were observed on the surface after 1300 min annealing (Figure 4c). The undulations were up to 4 μm long and eradicated any shallow surface scratches that were present before annealing. In some cases, the undulations even bridged deeper polishing scratches (black star in Figure 5). The extent of undulation formation, that is, height and density, varied across the surface, producing the large standard deviation (1.9 nm) in Figure 3 for these samples. However, the undulations were consistently aligned across the extent of the surface regardless of their density or size. The initial production of undulations could be observed within 60 min. Unlike previous experiments, the R_q value showed an increase with time between the different measurements during the duration of the experiment, implying that the system may not have reached steady state across the entire surface. However, the undulating surface features correspond to those predicted by Herring[31] based on the free energies of crystal surfaces produced during annealing indicating that this structure is representative of equilibrated surfaces at high temperatures. EBSD analysis of the surface after the experiments showed sharp Kikuchi lines of olivine in the same orientation as the underlying crystal for the undulations indicating that they are also composed of olivine (Figure 6).

Experiments with San Carlos Olivine ($Mg_{0.8}Fe_{0.2}SiO_4$): Oxidation Test. A San Carlos olivine crystal annealed at 900 °C under a gas mix of 1:9 CO/CO_2 ($fO_2 = 10^{-12.8}$ bars) showed evidence of surface oxidation by a change in color from light green to brown, despite still being in the olivine stability field (e.g., Nakamura and Schmalzried[32]). AFM observations of the mineral surface showed that it was covered in a new layer of material after 10 min in the oven. After oxidation, the surface

DOI: 10.1021/acsearthspacechem.6b00016
ACS Earth Space Chem. 2017, 1, 113−121

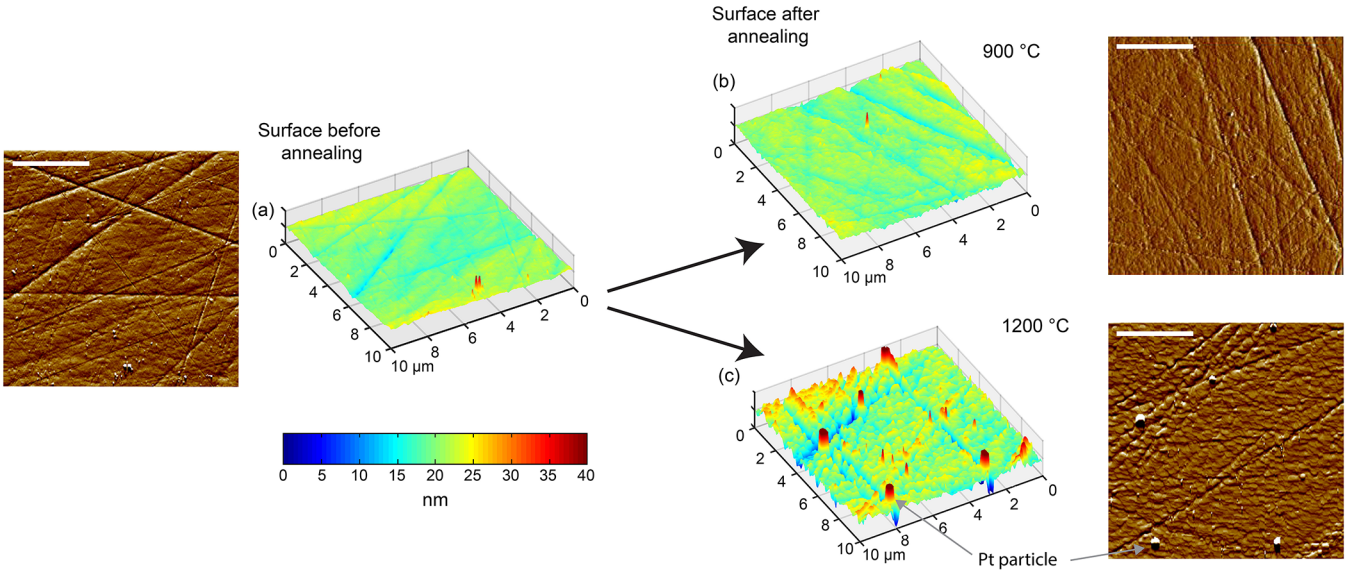

Figure 2. AFM deflection images and 3D plots of forsterite (Mg_2SiO_4) surface topography, where the before image (a) shows the presence of some scratches formed during the polishing procedure. (b) Surface annealed for 5000 min at 900 °C. (c) After 2 h of annealing at 1200 °C, the surface has clearly become rougher with some larger islands. Pt particles can be observed on the surface with a height larger than 40 nm, however, to keep the z color scale consistent between the images they are shown only up to a height of 40 nm. Scale bar in AFM deflection images: 2 μm.

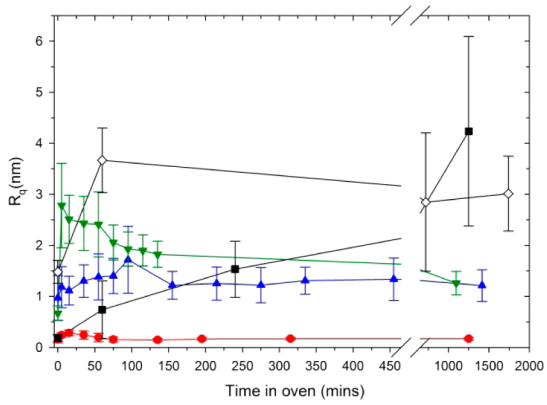

Figure 3. Change in surface roughness with time caused by annealing quartz, forsterite, and San Carlos olivine at 900 or 1200 °C: Quartz (red circles) at 900 °C, synthetic forsterite at 900 °C (blue triangles) and 1200 °C (downward pointing green triangles), San Carlos olivine at 900 °C (open diamonds) and 1200 °C (black squares). Error bars show the 1σ standard deviation of roughness measurements taken from 20 randomly chosen areas of the surface.

consisted of large mounds all aligned with an elongated axis in the same direction across the surface (Figure 1c). The mounds had a rough, textured surface and varied in size between 250 and 500 nm length with a height of up to 20 nm. In the EBSD analysis, no Kikuchi lines were observed indicating that the material was probably not olivine and was either amorphous or too rough for EBSD analysis. Absence of oxidation during the experiments under a 1:1 CO/CO_2 gas mix is thus expected due to the lack of color change after the experiments. The AFM observations also showed that the oxidation related surface topography was not observed during the more reducing experiments.

Quartz Experiment. The quartz experiments were difficult to conduct because the crystals had a tendency to crack during the first few minutes of the experiment as the crystal was heated across the α- to β-quartz phase transition. Typically the crystals broke so that they could no longer be easily analyzed using AFM. However, one experiment conducted at 900 °C produced a useable crystal that could be imaged. Nanometer observations of the sample surface indicated that discrete Pt particles, similar to those observed during the synthetic forsterite experiments, were detected. Therefore, these were avoided during the surface roughness analysis. Similar to the trend observed with the olivine crystals, an initial increase in the roughness was observed on the quartz surface during the first few minutes of the experiment (Figure 3). This roughness stabilized and coarsened during the following ~50 min until it had established a constant topography for the remainder of the experiment. Thus, it is expected that the surface had reached a steady-state structure that showed almost no change in surface topography compared to the initial surface. Unlike the synthetic forsterite, the quartz surface showed a much more limited change in the surface structure producing none of the undulations observed on forsterite or olivine, as is reflected in the very small R_q value measured at all time points on this surface. The surface topography was consistent across the surface and showed no undulations, reflected in the standard deviation of the R_q parameter, represented in the graph as error bars that are mostly smaller than the symbol for the quartz sample.

Testing for Increased Reactivity to Gases. A simple test for increased reactivity was conducted by leaving the annealed crystals exposed to air for 24 h after the experiment and then examining the surface using the AFM. All of the reacted olivine crystals demonstrated that they had begun to react with atmospheric gases as a layer formed on the surfaces that could be moved by the AFM tip. The exception to this was the highly reconstructed San Carlos olivine surface produced during experiments at 1200 °C. This surface showed reaction mainly on the tips of the undulations, where a similar smearing of the AFM image was observed as the tip moved a newly reacted layer. This texture was not observed on the polished surfaces before the experiments despite being left to react with the atmosphere for a number of days.

DOI: 10.1021/acsearthspacechem.6b00016
ACS Earth Space Chem. 2017, 1, 113−121

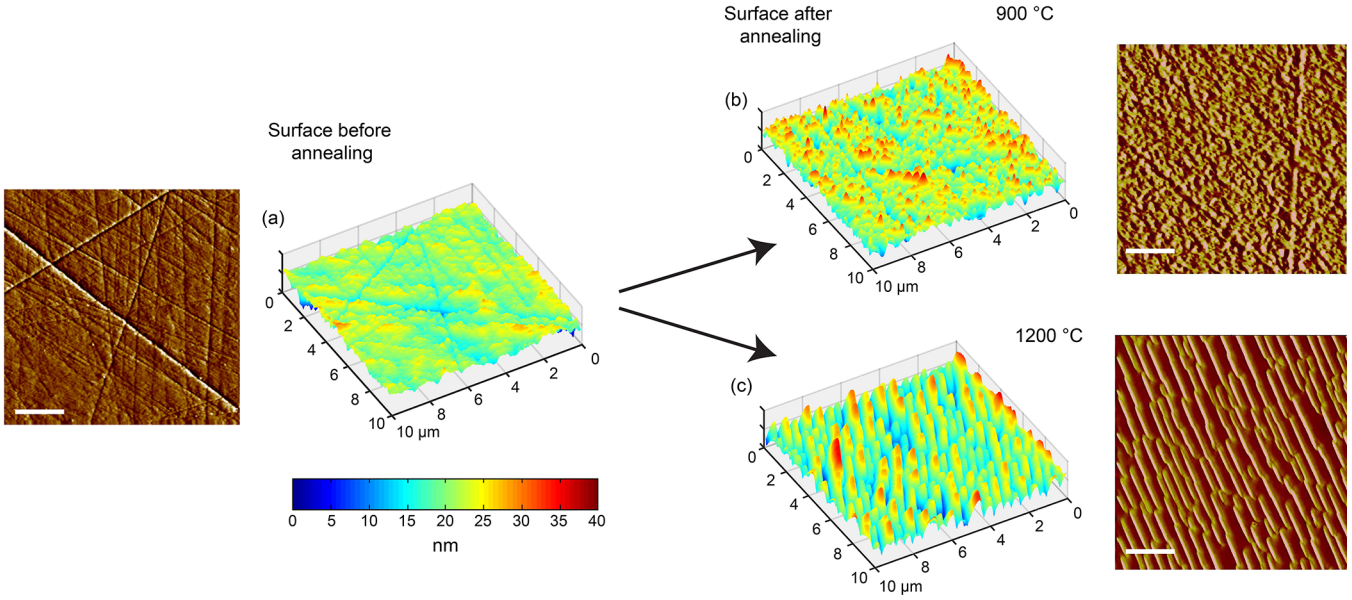

Figure 4. Three-dimensional plots of San Carlos olivine ($Mg_{1.8}Fe_{0.2}SiO_4$) surface topography. Scratches are present on the surfaces before annealing (a) along with some areas of slightly higher topography. (a) A typical example of an original surface from the 1200 °C experiment; different crystals were used for the experiments at the two different temperatures. These areas of higher topography are aligned with the polishing scratches. (b) After annealing at 900 °C for 1750 min, the surface has a clear increase in roughness with the formation of small islands. Some scratches are still present on the surface, however the roughness islands now have an orientation unrelated to the scratch orientations. (c) When San Carlos is annealed at 1200 °C for 1300 min, orientated undulations are visible on the surface reaching up to 40 nm in height. Evidence of original scratches is minimal. Scale bar in AFM deflection images is 2 μm.

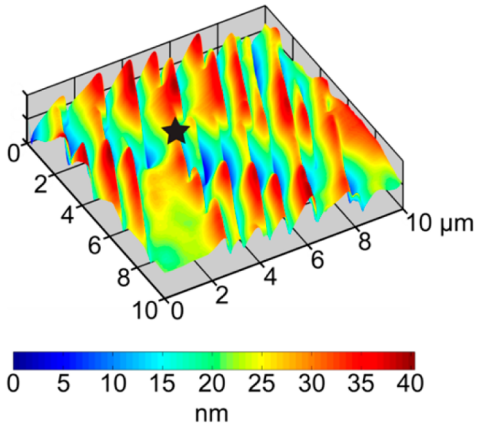

Figure 5. Three-dimensional plot of surface topography from a surface annealed at 1200 °C for 1300 min. The darker area running across the center of the plot is a previous scratch on the surface.

Intrinsic Material Property versus Contamination. Contaminants produced on the surface during the course of the experiments, such as the deposition of Pt or alumina, were clearly distinguishable from the underlying surface feature changes (Figure 1). However, polishing a crystal is also known to change the surface reactivity[33] through the formation of defects,[34] thus the effect of polishing should be considered when examining the structures produced during the experiments. Shallow scratches were present on the mineral surface after fine polishing with colloidal silica, as observed in the AFM measurements (for example, Figures 2a and 4a) and may have provided possible sites for evaporation and reconstruction during the high-temperature experiments. However, Figure 2c shows that the majority of the reconstruction on the surface is formed between the scratches (observable as linear features in the plot that have a dark blue color). Figure 5 further demonstrates that the prominent ridges produced at 1200 °C developed an orientation unrelated to a polishing scratch and in some cases even formed across a deep scratch in the surface (black star in Figure 5). This evidence shows that the formation of these orientated surface reconstructions is an intrinsic property of the surface rather than related to the formation of scratches at the same surface. Similarly the observation of Kikuchi lines both before and after the experiments indicates that the undulations consist of the same composition as the underlying olivine as EBSD is a surface sensitive technique that should only analyze within the width of the electron beam that has penetrated a limited distance (on the order of a few nanometers) into the surface[35,36] whereas the surface reconstruction can reach up to 40 nm in height (Figures 4c and 5). This also suggests that the highly deformed region reported previously in transmission electron microscopy studies[34] up to 100 nm into the sample surface is not present in our samples. In addition, no major changes in the quartz surface prepared using the same method was observed. Presolar dust grains have been shown to contain many dislocations[37] and thus the polished surfaces are a good comparison for processes occurring at highly reactive mineral surfaces found in the solar nebula.

Formation Mechanisms of Surface Undulations. Polished San Carlos olivine was more reactive than its Mg-pure forsterite counterpart, showing a much greater degree of surface rearrangement both in the 900 and 1200 °C experiments (Figures 4 and 5). Thus, the more complex chemistry associated with San Carlos olivine is confirmed to have a large effect on its surface reactivity. This is consistent with known changes in surface reactivity associated with dopants and chemical variations during grain boundary formation in mineral and metal systems.[38] Similar undulating and mound features to those observed at 1200 °C on the San

DOI: 10.1021/acsearthspacechem.6b00016
ACS Earth Space Chem. 2017, 1, 113−121

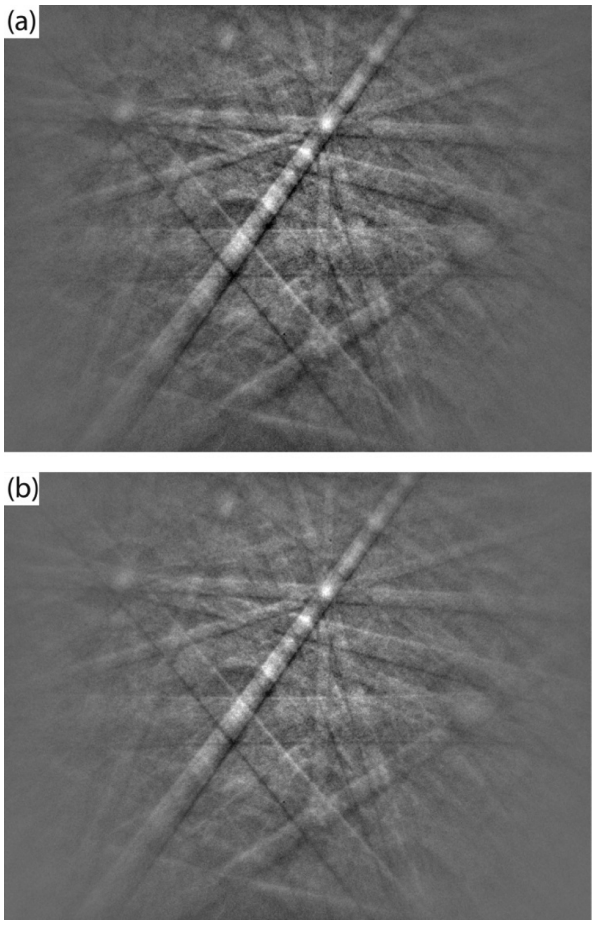

Figure 6. Electron backscattered diffraction patterns taken from the surface of the San Carlos olivine sample before the experiment (a) and after experiment at 1200 °C (b) where the large undulations could be observed using the atomic force microscope. The pattern indicates that the undulations are still olivine and have the same orientation as the original olivine material.

Carlos olivine have been documented at the surfaces of various materials in the thin film literature.[39,40] Their formation is attributed to mass diffusion during annealing,[41] hence, the ordered surface structure observed on the olivine surfaces will be controlled by the ability of atoms to diffuse across the surface at different temperatures and is an effect that would be expected on many different mineral surfaces. The underlying mineral structure clearly acts as a template for the growth of the mound structures as the surface retained the same Kikuchi lines (Figure 6) and thus the underlying crystalline orientation. This means that the mineral surface is expected to be a highly dynamic and complex system during high-temperature heating events where atoms can readily diffuse across the surface to grow as islands of new crystalline material.

Surface Reactivity and Gas Adsorption. The formation of the undulation texture increases the surface area available for gas adsorption as well as providing fresh, chemically active surfaces. Using the AFM height images and analysis software, topography measurements were conducted on samples using values stored on a regular grid. A global triangulation of these points was carried out using a MATLAB code and the area of each triangle was measured as the Euclidean norm of the cross product of the vectors constituting the triangle. All areas were then summed to arrive at a total surface area. The results of the calculations for the two San Carlos experiments, which showed the most significant surface changes and are most compositionally relevant for nebula processes, show that a 10 × 10 μm surface was increased by 10^5 nm^2 during San Carlos olivine surface reconstruction experiments at 1200 °C compared to the original polished surfaces, giving an increase of just 0.1%.

To estimate how this change in surface area may affect the ability of the surface to adsorb gas particles, we have used a Langmuir isotherm to calculate a monolayer of gas coverage. For simplicity, we calculated the weight of gas adsorbed as a complete monolayer for an area 10 × 10 μm (the area imaged by the AFM) with the different surface areas calculated from real surface roughness by rearranging the equation used to determine surface area from Langmuir isotherms

$$S_1 = \frac{W_m \bar{N} A_x}{\bar{M}} \quad (2)$$

to

$$W_m = \frac{S_1 \bar{M}}{\bar{N} A_x} \quad (3)$$

where S_1 is the sample surface area, W_m is the weight of gas adsorbed in a complete monolayer, $\bar{N}$ is Avogadro's number, and A_x and $\bar{M}$ are the cross-sectional area on the surface and weight of a water molecule, 10.8 Å^2 and 18.015 g/mol, respectively.[42] The samples with higher surface area show a similar change in the number of adsorption sites, increasing by 0.1% (10^8 sites) in our example area. Therefore, the number of adsorption sites is not expected to significantly increase through surface rearrangement. However, rounded structures at the atomic scale are modeled using multiple steps terminated along different planes within the structure, for example, in metal systems.[43] Thus, the formation of undulations at the mineral surface will produce defective and therefore highly reactive sites that would be readily available for gas adsorption. Considerations of crystal surface free energies predicts that these hill–valley structures will be formed during annealing of crystalline material where the surfaces present are different from the faces found on the predicted equilibrium crystal.[31] Therefore, such surface features would be expected to form at the surfaces of crystalline materials, such as olivine, present in the nebula if high enough temperatures are reached that remain below their melting temperature.

CONCLUSIONS

Adsorption onto mineral surfaces enables a variety of processes occurring in the solar nebula.[44] Our experiments show that surfaces of mineral grains are highly dynamic environments at high temperatures, promoting transport and redistribution of elements within a short time frame. Even large mineral dust grains with an extensive underlying crystalline structure can undergo significant surface rearrangement when exposed to short bursts of high temperature below their evaporation and melting temperatures. The similarity in surface structures observed both at the highest temperature (1200 °C) with forsterite and the annealed San Carlos olivine indicates that the surfaces evolve toward an undulating surface structure, predicted by crystal surface free energies[31] with the final structure reached at steady state being dependent on the system temperature and the reactivity of the material. Surfaces of mineral dust grains are therefore expected to react to high energy bursts of radiation in the solar nebulae and hence retain

DOI: 10.1021/acsearthspacechem.6b00016
ACS Earth Space Chem. 2017, 1, 113–121

defective and high energy sites that have been shown to be critical for volatile adsorption.[7]

The results of our study also demonstrate that surface reconstruction would be expected to be a common feature during other high-temperature experiments, for example, diffusivity experiments for magmatic processes related to olivine that typically have a temperature range of 800−1500 °C.[45−47] Surface reconstruction will provide fast routes for the incorporation of new species that are not dependent on bulk crystal properties. This may help to explain the discrepancies observed between short diffusion profiles measured with Rutherford backscattering spectrometry and longer profiles obtained using laser-ablation inductively coupled plasma mass spectrometry, an ongoing debate in the diffusivity community.[48] EBSD cannot be used as a tool to identify whether surface reconstruction has occurred, as it will produce the same EBSD pattern as the original material. Only with careful examination across a surface using AFM, as soon as the crystal is removed from the oven, can the surface features be distinguished and analyzed. Other species are also mobile at these high temperatures, including alumina, that can readily be deposited on the surface of exposed crystals within an oven.

AUTHOR INFORMATION

Corresponding Author

*E-mail: h.e.king@uu.nl.

ORCID

Helen E. King: 0000-0002-1825-782X

Present Address

(H.E.K.) Department of Earth Sciences, Utrecht University, Budapestlaan 4, 3584 CD Utrecht, The Netherlands.

Author Contributions

The manuscript was written through contributions of all authors. All authors have given approval to the final version of the manuscript.

Notes

The authors declare no competing financial interest.

ACKNOWLEDGMENTS

This work was funded by a Deutsche Forschungsgemeinsschaft grant awarded to A. Putnis (PU153/16-1) and a Humboldt fellowship funding a short stay for H.St.C.O. at the University of Münster, Germany. All analytical and experimental procedures were carried out at the Institut für Mineralogie, University of Münster, Germany. H.E.K. acknowledges funding through the European Marie Curie Actions International Outgoing Fellowship (TMuPiFe 2012-328731). O.P. acknowledges The Netherlands Organisation for Scientific Research (NWO) Veni Grant (No. 863.13.006). C.V.P. and A.P. acknowledge funding through the EU Marie Curie International Training Networks, CO2REACT, FlowTrans and MINSC. The authors thank C. H. Wijbrans. for advice with the experimental work and I. L. ten Kate as well as two anonymous reviewers and Dr. J. Nuth for their comments on the manuscript.

REFERENCES

(1) van Dishoeck, E. F.; Bergin, E. A.; Lis, D. C.; Lunine, J. I. Water: From clouds to planets. In *Protostars and Planets VI*; Beuther, H., Klessen, R., Dullemond, C., Henning, T., Eds.; University of Arizona Press, 2014; pp 835−858.

(2) Morbidelli, A.; Chambers, J.; Lunine, J.; Petit, J.; Robert, F.; Valsecchi, G.; Cyr, K. Source regions and time scales for the delivery of water to Earth. *Meteorit. Planet. Sci.* **2000**, *35*, 1309−1320.

(3) Alexander, C. O.; Bowden, R.; Fogel, M.; Howard, K.; Herd, C.; Nittler, L. The provenances of asteroids, and their contributions to the volatile inventories of the terrestrial planets. *Science* **2012**, *337*, 721−723.

(4) Altwegg, K.; Balsiger, H.; Bar-Nun, A.; Berthelier, J.; Bieler, A.; Bochsler, P.; Briois, C.; Calmonte, U.; Combi, M.; De Keyser, J. 67P/Churyumov-Gerasimenko, a Jupiter family comet with a high D/H ratio. *Science* **2015**, *347*, 1261952.

(5) Asaduzzaman, A. M.; Laref, S.; Deymier, P. A.; Runge, K.; Cheng, H. P.; Muralidharan, K.; Drake, M. J. A first-principles characterization of water adsorption on forsterite grains. *Philos. Trans. R. Soc., A* **2013**, *371*, 20110582.

(6) Downing, C. A.; Ahmady, B.; Catlow, C. R.; de Leeuw, N. H. The interaction of hydrogen with the {010} surfaces of Mg and Fe olivine as models for interstellar dust grains: a density functional theory study. *Philos. Trans. R. Soc., A* **2013**, *371*, 20110592.

(7) King, H.; Stimpfl, M.; Deymier, P.; Drake, M.; Catlow, C.; Putnis, A.; de Leeuw, N. Computer simulations of water interactions with low-coordinated forsterite surface sites: implications for the origin of water in the inner solar system. *Earth Planet. Sci. Lett.* **2010**, *300*, 11−18.

(8) Vattuone, L.; Smerieri, M.; Savio, L.; Asaduzzaman, A. M.; Muralidharan, K.; Drake, M. J.; Rocca, M. Accretion disc origin of the Earth's water. *Philos. Trans. R. Soc., A* **2013**, *371*, 20110585.

(9) Hallis, L. J.; Huss, G. R.; Nagashima, K.; Taylor, G. J.; Halldorsson, S. A.; Hilton, D. R.; Mottl, M. J.; Meech, K. J. Evidence for primordial water in Earth's deep mantle. *Science* **2015**, *350*, 795−797.

(10) Hill, H. G.; Nuth, J. A. The catalytic potential of cosmic dust: implications for prebiotic chemistry in the solar nebula and other protoplanetary systems. *Astrobiology* **2003**, *3*, 291−304.

(11) Henning, T. Cosmic silicates. *Annu. Rev. Astron. Astrophys.* **2010**, *48*, 21−46.

(12) Nagahara, H.; Kushiro, I.; Mysen, B. O. Evaporation of olivine: Low pressure phase relations of the olivine system and its implication for the origin of chondritic components in the solar nebula. *Geochim. Cosmochim. Acta* **1994**, *58*, 1951−1963.

(13) Yamada, M.; Tachibana, S.; Nagahara, H.; Ozawa, K. Anisotropy of Mg isotopic fractionation during evaporation and Mg self-diffusion of forsterite in vacuum. *Planet. Space Sci.* **2006**, *54*, 1096−1106.

(14) Wang, J.; Davis, A. M.; Clayton, R. N.; Hashimoto, A. Evaporation of single crystal forsterite: Evaporation kinetics, magnesium isotope fractionation, and implications of mass-dependent isotopic fractionation of a diffusion-controlled reservoir. *Geochim. Cosmochim. Acta* **1999**, *63*, 953−966.

(15) Grossman, L.; Larimer, J. W. Early chemical history of the solar system. *Rev. Geophys.* **1974**, *12*, 71−101.

(16) Saxena, S. K.; Eriksson, G. Chemistry of the formation of the terrestrial planets. In *Chemistry and Physics of Terrestrial Planets*; Saxena, S. K., Ed.; Springer, 1986; pp 30−105.

(17) Sunshine, J. M.; Pieters, C. M. Determining the composition of olivine from reflectance spectroscopy. *J. Geophys. Res.- Planets* **1998**, *103*, 13675−13688.

(18) Kaito, C.; Ojima, Y.; Kamitsuji, K.; Kido, O.; Kimura, Y.; Suzuki, H.; Sato, T.; Nakada, T.; Saito, Y.; Koike, C. Demonstration of crystalline forsterite grain formation due to coalescence growth of Mg and SiO smoke particles. *Meteorit. Planet. Sci.* **2003**, *38*, 49−57.

(19) Rietmeijer, F. J.; Hallenbeck, S. L.; Nuth, J. A.; Karner, J. M. Amorphous magnesiosilicate smokes annealed in vacuum: the evolution of magnesium silicates in circumstellar and cometary dust. *Icarus* **2002**, *156*, 269−286.

(20) Harker, D. E.; Desch, S. J. Annealing of silicate dust by nebular shocks at 10 AU. *Astrophys. J.* **2002**, *565*, L109.

(21) Connolly, H. C., Jr; Love, S. G. The formation of chondrules: petrologic tests of the shock wave model. *Science* **1998**, *280*, 62−67.

DOI: 10.1021/acsearthspacechem.6b00016
ACS Earth Space Chem. 2017, 1, 113−121

(22) Nagahara, H.; Ozawa, K. Mechanism of forsterite evaporation as inferred from surface microstructures. *Proc. Jpn. Acad., Ser. B* **1999**, *75*, 29−34.
(23) Boss, A. P. A Concise Guide to Chondrule Formation Models. In *Chondrules and the protoplanetary disk*; Cambridge University Press, 1996; pp 257.
(24) Zhukova, I.; O'Neill, H. S.; Cambell, I. H.; Kilburn, M. R. The effect of silica activity on the diffusion of Ni and Co in olivine. *Contrib. Mineral. Petrol.* **2014**, *168*, 1−15.
(25) Jollands, M. C.; O'Neill, H. S. C.; Hermann, J. The importance of defining chemical potentials, substitution mechanisms and solubility in trace element diffusion studies: the case of Zr and Hf in olivine. *Contrib. Mineral. Petrol.* **2014**, *168*, 1−19.
(26) Xu, Y.; Shankland, T. J.; Linhardt, S.; Rubie, D. C.; Langenhorst, F.; Klasinski, K. Thermal diffusivity and conductivity of olivine, wadsleyite and ringwoodite to 20 GPa and 1373 K. *Phys. Earth Planet. Inter.* **2004**, *143-144*, 321−336.
(27) O'Neill, H. S. C.; Berry, A. J. Activity coefficients at low dilution of CrO, NiO and CoO in melts in the system CaO−MgO−Al_2O_3−SiO_2 at 1400 C: using the thermodynamic behaviour of transition metal oxides in silicate melts to probe their structure. *Chem. Geol.* **2006**, *231*, 77−89.
(28) Prior, D. J.; Boyle, A. P.; Brenker, F.; Cheadle, M. C.; Day, A.; Lopez, G.; Peruzzo, L.; Potts, G. J.; Reddy, S.; Spiess, R. The application of electron backscatter diffraction and orientation contrast imaging in the SEM to textural problems in rocks. *Am. Mineral.* **1999**, *84*, 1741−1759.
(29) Jehn, H. High temperature behaviour of platinum group metals in oxidizing atmospheres. *J. Less-Common Met.* **1984**, *100*, 321−339.
(30) Kolobov, A.; Wilhelm, F.; Rogalev, A.; Shima, T.; Tominaga, J. Thermal decomposition of sputtered thin PtOx layers used in super-resolution optical disks. *Appl. Phys. Lett.* **2005**, *86*, 121909.
(31) Herring, C. Some theorems on the free energies of crystal surfaces. *Phys. Rev.* **1951**, *82*, 87.
(32) Nakamura, A.; Schmalzried, H. On the nonstoichiometry and point defects of olivine. *Phys. Chem. Miner.* **1983**, *10*, 27−37.
(33) MacInnis, I. N.; Brantley, S. L. The role of dislocations and surface morphology in calcite dissolution. *Geochim. Cosmochim. Acta* **1992**, *56*, 1113−1126.
(34) Pinilla, C.; Davis, S. A.; Scott, T. B.; Allan, N. L.; Blundy, J. D. Interfacial storage of noble gases and other trace elements in magmatic systems. *Earth Planet. Sci. Lett.* **2012**, *319-320*, 287−294.
(35) Winkelmann, A. Principles of depth-resolved Kikuchi pattern simulation for electron backscatter diffraction. *J. Microsc.* **2010**, *239*, 32−45.
(36) Zaefferer, S. On the formation mechanisms, spatial resolution and intensity of backscatter Kikuchi patterns. *Ultramicroscopy* **2007**, *107*, 254−266.
(37) Lodders, K.; Amari, S. Presolar grains from meteorites: Remnants from the early times of the solar system. *Chem. Erde* **2005**, *65*, 93−166.
(38) Rohrer, G. S. Grain boundary energy anisotropy: a review. *J. Mater. Sci.* **2011**, *46*, 5881.
(39) Orme, C.; Johnson, M.; Leung, K.; Orr, B. Atomic force microscopy and scanning tunneling microscopy studies of large-scale unstable growth formed during GaAs (001) homoepitaxy. *Mater. Sci. Eng., B* **1995**, *30*, 143−148.
(40) Orme, C.; Johnson, M.; Sudijono, J.; Leung, K.; Orr, B. Large scale surface structure formed during GaAs (001) homoepitaxy. *Appl. Phys. Lett.* **1994**, *64*, 860−862.
(41) Gao, H.; Nix, W. D. Surface roughening of heteroepitaxial thin films. *Annu. Rev. Mater. Sci.* **1999**, *29*, 173−209.
(42) Livingston, H. The cross-sectional areas of molecules adsorbed on solid surfaces. *J. Colloid Sci.* **1949**, *4*, 447−458.
(43) Jeong, H.; Williams, E. D. Steps on surfaces: experiment and theory. *Surf. Sci. Rep.* **1999**, *34*, 171−294.
(44) Dulieu, F.; Congiu, E.; Noble, J.; Baouche, S.; Chaabouni, H.; Moudens, A.; Minissale, M.; Cazaux, S. How micron-sized dust particles determine the chemistry of our Universe. *Sci. Rep.* **2013**, *3*, 1338.
(45) Spandler, C.; O'Neill, H. S. C. Diffusion and partition coefficients of minor and trace elements in San Carlos olivine at 1,300 C with some geochemical implications. *Contrib. Mineral. Petrol.* **2010**, *159*, 791−818.
(46) Chakraborty, S. Rates and mechanisms of Fe-Mg interdiffusion in olivine at 980−1300 C. *J. Geophys. Res.- Sol. Ea.* **1997**, *102*, 12317−12331.
(47) Cherniak, D. REE diffusion in olivine. *Am. Mineral.* **2010**, *95*, 362−368.
(48) Watson, E.; Cherniak, D.; Thomas, J.; Hanchar, J.; Wirth, R. Crystal surface integrity and diffusion measurements on Earth and planetary materials. *Earth Planet. Sci. Lett.* **2016**, *450*, 346−354.

DOI: 10.1021/acsearthspacechem.6b00016
ACS Earth Space Chem. 2017, 1, 113−121